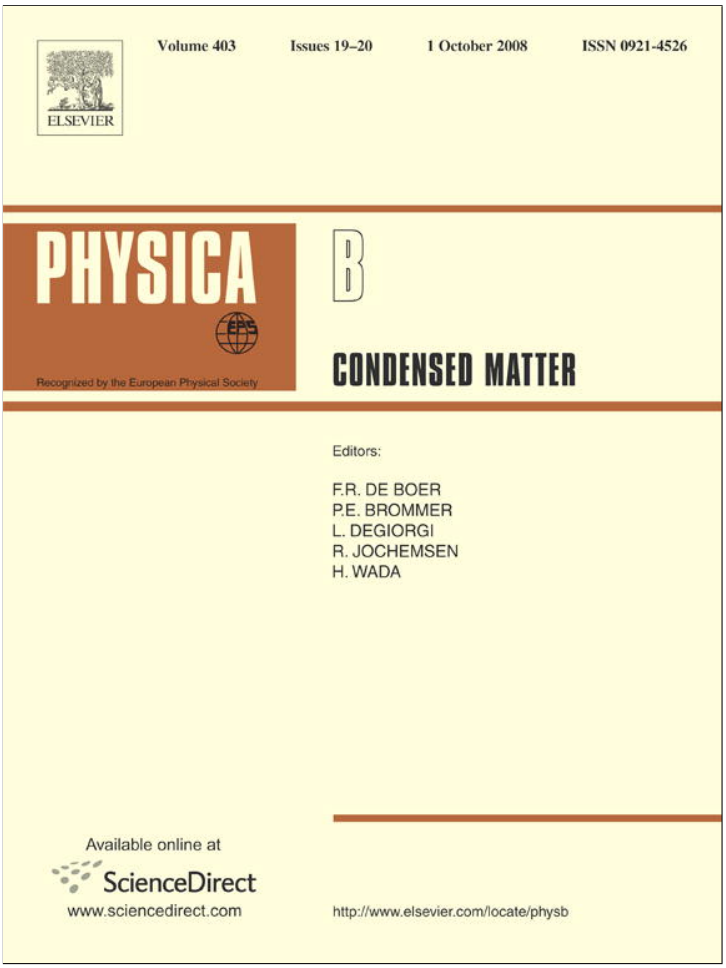

Physica B 403 (2008) 3585–3588

Contents lists available at ScienceDirect

Physica B

journal homepage: www.elsevier.com/locate/physb

Anomalous temperature dependence of optical properties of cubic MgZnO: Effect of carrier localization

H.P. Zhou [a,*], M. Xu [a], W.Z. Shen [b]

[a] Laboratory for Low-dimensional Structure Physics, Institute of Solid State Physics and School of Physics and Electronic Engineering, Sichuan Normal University, 5 Jing'an Road, Chengdu 610068, PR China

[b] Laboratory of Condensed Matter Spectroscopy and Opto-Electronic Physics, Department of Physics, Shanghai Jiao Tong University, 1954 Hua Shan Road, Shanghai 200030, PR China

ARTICLE INFO

Article history:
Received 7 May 2008
Accepted 27 May 2008

PACS:
78.66.Hf
78.20.Ci
78.40.Fy
78.40.Pg

Keywords:
MgZnO thin films
Carrier localization
Optical properties

ABSTRACT

We investigated the temperature-dependent optical transmission spectra in reactive-electron-beam-evaporation (REBE)-grown cubic MgZnO thin films and extracted the band gap E_g, broadening factor and refractive index. Incomplete and complete "S-shaped" thermal dependence of E_g are observed in $Mg_{0.77}Zn_{0.23}O$ and $Mg_{0.55}Zn_{0.45}O$, respectively. This behavior is caused by carrier localization induced by potential fluctuation or possible other disorder mechanisms, such as phase separation and phase transition. Also, the broadening factor and refractive index exhibit similar anomalous temperature dependence, supporting the occurrence of carrier localization. Furthermore, the magnitude of carrier localization was estimated by simulating the anomalous behaviors of E_g with different models.

1. Introduction

As a wide-band-gap semiconductor material, ZnO (E_g~3.37 eV) with pronounced advantage of large exciton binding energy (~60 meV) has been recognized as a promising candidate to compete with GaN for the development of short-wavelength photoelectronic devices. An important step in order to design ZnO-based photoelectronic device is the realization of band gap engineering to create barrier layers and quantum wells in devices heterostructures. Incorporation of cadmium into ZnO results in band gap narrowing. However, alloying with MgO leads to increase of band gap. Therefore MgZnO is an appreciable candidate as barrier material for ZnO quantum wells and seems well suited for more sophisticated structures such as waveguides or distributed Bragg reflectors [1]. Ohtomo et al. [2] reported the first synthesis of high-quality, single hexagonal phase $Mg_xZn_{1-x}O$ thin film with Mg concentration x up to 33 at% due to nonequilibrium nature of the pulsed laser deposit (PLD) growth. Above 33 at%, MgO will segregate from the wurtzite MgZnO lattice. The structural transition from hexagonal to cubic phase has been observed in PLD-grown MgZnO with Mg content greater than 45 at%, and the single cubic phase $Mg_xZn_{1-x}O$ thin films are obtained with x in the range of 0.50–0.86 [3] and 0.82–1.00 [4]. Authors of this work and their collaborators have reported the growth of cubic $Mg_xZn_{1-x}O$ thin films by a simple and low-cost method of reactive-electron-beam-evaporation (REBE) and analyzed the detailed Mg composition nonuniformity [5] and long-wavelength optical phonon properties [6].

In general, alloying may generate disorder and potential fluctuation, resulting in the increase of localization states in alloy semiconductors, where carriers feel different potential depending on the local concentration and/or arrangement of substituting elements. This effect is large in ZnO-based materials, because the Bohr radius of excitons in ZnO is as small as 1.8 nm, and the excitons are therefore more sensitive to local inhomogeneity [2]. Carrier localization introduced by disorder and potential fluctuation is extensively studied in nitride ternary, such as InGaN [7,8], AlGaN [9–11] and GaNAs [12]. However, there are few reports on the effect of carrier localization on optical properties for MgZnO (especially cubic MgZnO) up to now. J. Huso et al. [13] have observed an additional Raman mode at the low-frequency wing of LO spectral line of $Mg_{0.2}Zn_{0.8}O$ and assigned this mode to the effect of disorder. Pan et al. [14] have analyzed the Raman spectral

* Corresponding author. Tel.: +86 28 84760792; fax: +86 28 84760096.
E-mail address: haipzhou@sina.com (H.P. Zhou).

0921-4526/$ - see front matter © 2008 Elsevier B.V. All rights reserved.
doi:10.1016/j.physb.2008.05.034

broadening and asymmetry induced by potential fluctuation in $Mg_xZn_{1-x}O$ ($0 \leqslant x \leqslant 0.14$) nanopowders.

Recently, some exciting progresses in MgZnO-base devices have been made. For example, an $Mg_{0.3}Zn_{0.7}O$/ZnO heterostructure field-effect transistor has been demonstrated [15], and the enhancement of exciton binding energy has been shown in $Mg_{0.23}Zn_{0.77}O$/ZnO multiple QWS (59 meV for ZnO and 115 meV for the QWs) [16]. Carrier localization has a significant effect on the alloy-based optical devices, determining the emission energy in LED and contributing to optical gain within laser structures [17]. Therefore, gaining insight into the carrier location of MgZnO system is of both theoretical and substantial significance.

In this work, we have carried out a detailed investigation of temperature-dependent optical transmission spectra in REBE-grown cubic MgZnO thin films for the information of band gap and broadening factor, as well as the refractive index. Anomalous thermal behaviors of the band gap are obtained in both samples and simulated by different models. Furthermore, both the broadening factor and the refractive index exhibit anomalous temperature dependence. It is believed these results are caused by carrier localization induced by potential fluctuation or possible other disorder mechanisms, such as phase separation and phase transition.

2. Experiments

Both hexagonal and cubic MgZnO thin films were grown in a REBE system on fine-polished quartz or sapphire substrates at low temperature. The $(MgO)_x(ZnO)_{1-x}$ target was sintered at 1500 °C by blending the polycrystalline MgO and ZnO powder (each with the purity of 99.9%) into various ratios for the evaporation sources and further growth details are described in Ref. [18] and references therein. The ratio of Mg:Zn (at%) in the MgZnO film was surveyed through both the X-ray photoelectron spectroscopy and the transmission measurements [5]. In this work, we mainly focus on two samples: one is $Mg_{0.77}Zn_{0.23}O$ on quartz substrate (sample A) and the other $Mg_{0.55}Zn_{0.45}O$ on sapphire (sample B). The X-ray diffraction (XRD) measurements reveal existence of cubic phase signatures and absence of hexagonal phase signatures, demonstrating single cubic phase nature of the studied MgZnO samples [5,18]. The temperature-dependent optical transmission measurements were performed on the Jobin Yvon 460 monochromator under a Janis variable temperature [from 10 K to room temperature (RT)] closed-cycle refrigerator system [18,19].

3. Results and discussion

Fig. 1 shows the temperature-dependent optical transmission spectra of both samples at RT. The absorption edge of MgZnO samples is less distinct than that of pure ZnO due to alloying, as reported in Refs. [18,20]. As a consequence of different substrate and film thickness, two samples exhibit different optical transparence (both more than 80%). Compared with sample B, absorption edge of sample A locates in shorter wavelength range, indicating a larger band gap. Furthermore, for sample A, prominent Fabry–Perot interference fringes due to multiple layer-substrate reflections are observed in long-wavelength region, and vanish in the vicinity of band gap E_g of around 6.1–6.2 eV. The temperature-dependent band gap of MgZnO can be obtained by calculating the optical transmission (Tr) through the sigmoidal equation of the absorption coefficient $\alpha(E)$ [21]:

$$\alpha(E) = \alpha_0 \Big/ \left[1 + \exp\left(\frac{E_g - E}{\Delta E}\right)\right] \quad (1)$$

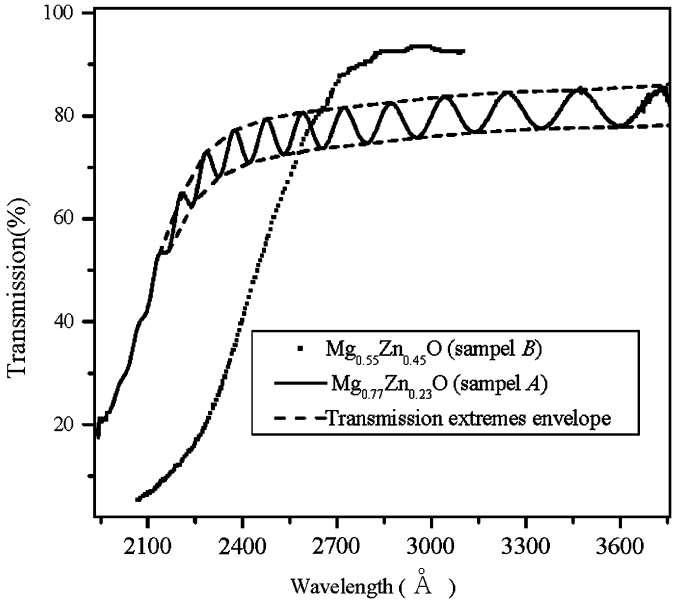

Fig. 1. Room temperature transmission spectra of sample A (solid curve) and sample B (dotted curve), together with the transmission extremes envelope (dashed curves).

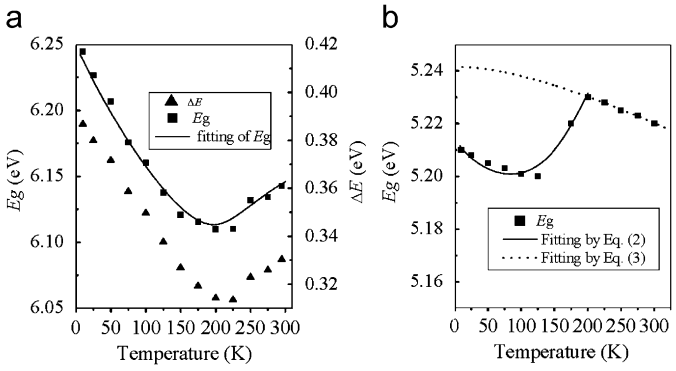

Fig. 2. (a) The band gap E_g (solid squares) and Urbach broadening factor ΔE (solid triangles) as a function of temperature in sample A. (b) The band gap E_g of sample B. The solid curve and dotted curve are the fitting results of E_g.

where α_0 is a fitting parameter and ΔE the Urbach broadening factor. Here the coefficient $\alpha(E)$ is correlated to transmission Tr by $\alpha(E) \propto -\ln(\mathrm{Tr})$, i.e., neglecting the interface reflection losses and optical scattering due to the high transmission in MgZnO.

Fig. 2(a) and (b) displays the temperature-dependent band gap E_g (solid squares) of sample *A* and sample B respectively. One can see that E_g of both MgZnO samples does not follow the usual behavior of a semiconductor band gap predicted by either the Varshni [22] or Bose–Einstein [23] formula. Instead, E_g of both samples exhibits an anomalous thermal behavior. For sample A, E_g shows a red shift up to 200 K, followed by a blue shift in the range of 200 K-RT. However, for sample B, when the temperature increases up to 125 K, an initial small decrease in E_g is observed, followed by an increase in the temperature range of 125–200 K, and finally E_g decreases again as the temperature increases above 200 K. This result is a so-called "S-shaped" dependence, which has been observed by means of photoluminescence or absorption in dilute nitrides such as AlGaN [10], GaAsN [12] and InGaN [21], and can be explained by the localization state due to alloy potential fluctuation or other disorder mechanism. It is worthy to note that, in comparison to sample B, sample A shows an incomplete

"S-shaped" (semi-S-shaped) dependence due to the carrier localization up to RT.

A complete "S-shaped" thermal behavior can be separated into three regions. At low-temperature region (10–200 K for sample A and 10–125 K for sample B) the band gap E_g slowly decreases due to the excitons being gradually trapped into low-energy localization states. As the temperature increases, E_g begins to increase in the second region (200 K-RT for sample A, and 125–200 K for sample B), as the excitons gain more thermal energy and are activated into higher localization state. Eventually, in the third region (above RT for sample A and out of the range of measurement, and 200 K-RT for sample B) excitons are completely delocalized, and hence, E_g shrinks as expected.

In Fig. 2(a), the temperature-dependent Urbach broadening factor ΔE of sample A is also given (solid triangles). Interestingly, both ΔE and E_g exhibit a similar trend and turning points at the same temperature of about 200 K. The larger Urbach energy (~350 meV) and similar trend of ΔE to E_g in Fig. 2(a), together with the observation of Mg composition nonuniformity in Ref. [5], indicate the more randomness in the alloy. In our previous work [19], we have qualitatively interpreted the anomalous dependence of ΔE and band gap E_g in sample A in terms of carrier localization due to potential fluctuation, a pronounced effect observed in MgZnO because of distinct band gap difference between ZnO and MgO [24]. A model taking into account the thermal activation and transfer of localized excitons is developed by Li et al. [7] to fit the blueshift of emission peak with temperature. In order to gain a deeper understanding of the effect of carrier localization in MgZnO, we adopt this model to quantitatively analyze the "semi-S-shaped" or "S-shaped" temperature dependence of E_g in both samples. The temperature-dependent band gap (or emission peak energy) can be obtained by solving the equation of $E(T)$:

$$\frac{E_0 - E}{k_B T} e^{(E_0 - E)/k_B T} = \left(\frac{\tau_r}{\tau_{tr}}\right)\left[\left(\frac{\sigma}{k_B T}\right)^2 - \frac{E_0 - E}{k_B T}\right] e^{(E_0 - E_a)/k_B T} \quad (2)$$

where E_0 and σ represent the center and width of localization state distribution function, respectively; τ_r and τ_{tr} the carrier recombination time and carrier transfer time, respectively; E_a and k_B a barrier level of localized state and Boltzmann constant, respectively. If the energy $E(T)$ value follows Eq. (2), it can be regarded as the band gap energy (or the emission peak energy) corresponding to a certain temperature T. The solid curve in Fig. 2(a) describes the fitting result of E_g for sample A, with the fitting parameters of $E_a = 6.253$ eV, $E_0 = 6.242$ eV, $\tau_r = 800$ ps, $\tau_{tr} = 0.03$ ps and $\sigma = 0.050$ eV. These parameter values are reasonable in physics. In this model, the value of $E_a - E_0$ (11 meV for sample A) can be used to estimate the magnitude of carrier localization.

Considering the presence of two turning points at about 125 and 200 K, respectively, mentioned above in $E_g(T)$ of sample B, we fit $E_g(T)$ in two different temperature ranges of 10–125 K and 125 K-RT by means of different models. In the range of 10–125 K, Eq. (2) is adopted again and the fitting results are shown in Fig. 2(b) (solid curve). It can be seen that the accuracy of this fitting is worse than that of sample A. It is noted that some fitting parameters (i.e., $E_a = 5.215$ eV, $E_0 = 5.368$ eV, $\tau_r = 0.2$ ps, $\tau_{tr} = 0.03$ ps and $\sigma = 0.050$ eV) seem unreasonable in this model. The value of $E_a - E_0$ is negative and does not reflect the barrier effect, sequentially, the magnitude of the carrier localization. As such, we suppose that there also exists other disorder mechanism to dominate the carrier localization in sample B. In fact, the composition of Mg extremely exceeds the solubility limit (~4%) of Mg into ZnO in cubic MgZnO. This implies that REBE is also a nonequilibrium method for the growth of cubic MgZnO. As a result, some disorder mechanisms such as phase separation and composition fluctuation are expected. Indeed, Choopun et al. [3] have found MgO separated from hexagonal MgZnO lattice with Mg composition of more than 33%. Additionally, the composition of Mg is 0.55 in sample B, which is near the transition point between hexagonal phase and cubic phase in MgZnO grown by REBE method [18]. So we can assume the occurrence of phase transition caused by the variation of temperature in sample B. The thermal behavior of E_g in the range of 10–200 K in sample B caused by the above disorder mechanisms cannot be precisely modeled using Eq. (2). However, we are able to estimate the magnitude of carrier localization by measuring the deviation of experimental E_g from the classical Varshni formula at low temperature [12,25]. In the range of 200 K-RT, instead of 10 K-RT, E_g is fitted by the Varshni formula

$$E_g(T) = E_g(0) - \frac{\alpha T^2}{\beta + T} \quad (3)$$

where the band gap $E_g(0) = 5.242$ eV at 0 K, $\alpha = 1.43 \times 10^{-4}$ eV/K, and $\beta = 300$ K. The fitting result is plotted in dotted curve in Fig. 2(b). Below 200 K, carrier is regarded as localized and above 200 K is fully delocalized and hence, the localization energy in sample B is of about 40 meV.

As discussed above, the Urbach broadening factor ΔE in Eq. (1) indicates the magnitude of randomness in the samples. We have summarized ΔE as a function of Mg composition x in Fig. 3. The solid circles denote ΔE of samples A and B, and the data marked by other symbols are from Refs. [5,26], in which Mg composition x is smaller than 0.36 and the MgZnO samples are in hexagonal phase. ΔE as a function of x can be fitted by a cubic relation of $\Delta E = a + bx + cx^2 + dx^3$ with constants of $a = 26.31$, $b = 245.96$, $c = -444.82$, $d = 821.50$. The fitting result is shown in Fig. 3 (solid curve). As composition x increases, ΔE increases monotonically from 31 meV ($x = 0$) to 150 meV ($x = 0.55$, sample B), and finally 330 meV ($x = 0.77$, sample A). However, we cannot simply conclude that the magnitude of carrier localization in sample A is stronger than that in sample B.

Another possible manifestation of carrier localization is the anomalous thermal behavior of refractive index. For sample A, the interference fringes in optical transmission spectra shown in Fig. 1 are beneficial to determine the refractive index n below the band gap and the thickness d. We studied the temperature coefficient of refractive index n of sample A on the basis of precise determina-

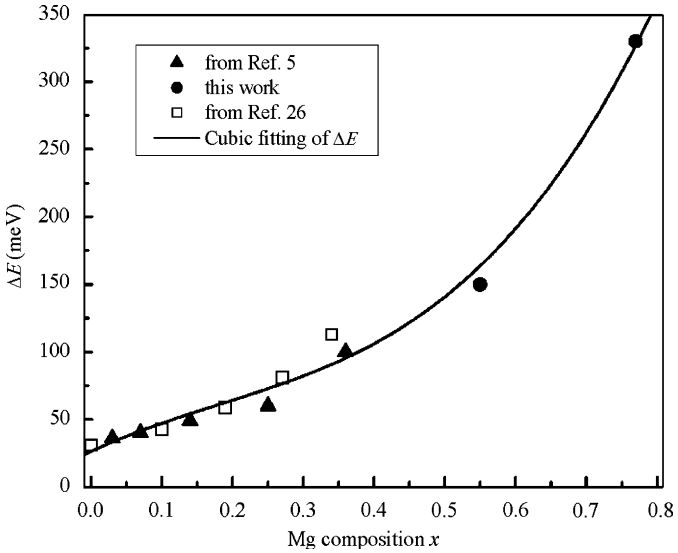

Fig. 3. Urbach broadening factor ΔE as a function of Mg composition x and its cubic relation fitting result (solid curve). Data from Refs. [5,26] and present work are shown as solid triangles, open squares and solid circles, respectively.

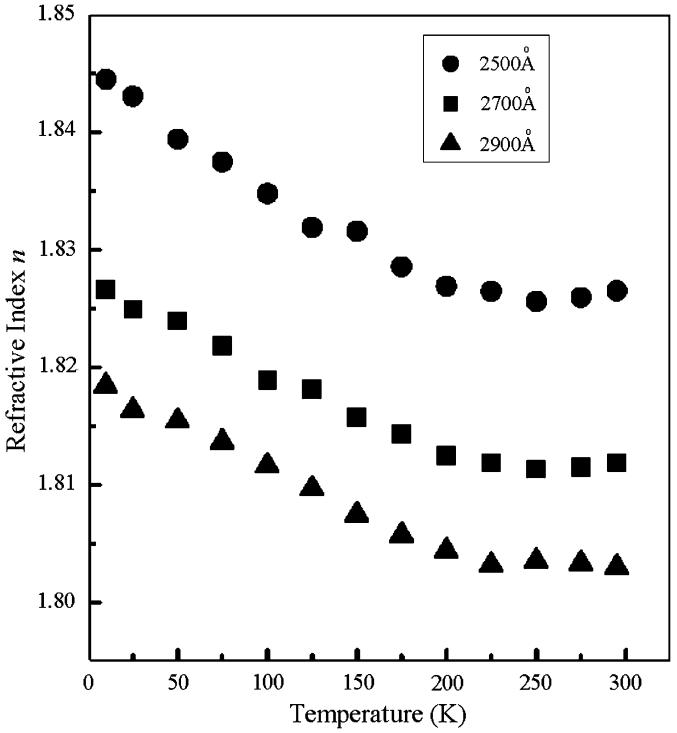

Fig. 4. Temperature-dependent refractive index n at several typical wavelengths. The refractive index sharply decreases with the increase of temperature in the range of 10–200 K and slightly increases above 200 K.

tion of n and d by the widely used envelope method established by Swanepoel. The validity of our procedure was confirmed by the yielded half integer or integer order of extremes [19]. The envelopes of the transmission extremes at RT have been typically shown as the dashed curves in Fig. 1. The obtained refractive index data of 1.806–1.834 at RT is well between those of $Mg_{0.36}Zn_{0.64}O$ and MgO [20]. The wavelength-dependent refractive indices at various temperatures have been further described by the classical Sellmeier law for the continuous refractive index dispersion in sample A. Fig. 4 illustrates the temperature-dependent refractive index n (solid points) at various wavelengths (λ) from the Sellmeier law. At a given wavelength (photon energy), the refractive index sharply decreases with the increase of temperature in the range of 10–200 K, which reveals a negative value for the temperature coefficient dn/dT. On the contrary, the refractive index slightly increases above 200 K, indicating a small positive dn/dT. It should be noted that refractive index n and band gap E_g (see Fig. 2(a)) present turning points at the same temperature of about 200 K. In our previous work [19], we have pointed out that dn/dT is closely correlated to dE_g/dT and developed a model to simulate dn/dT, in which dE_g/dT plays a key role. It is believed that the anomalous thermal behavior of refractive index is relevant with above "semi-S-shaped" behavior of E_g resulting from disorder state.

4. Conclusion

In summary, we have employed temperature-dependent optical transmission spectra to extract band gap energy, broadening factor and refractive index, as well as their temperature dependence in cubic MgZnO thin films grown by REBE. "Semi-S-shaped" and complete "S-shaped" thermal behavior of the band gap E_g are observed. In addition, both the broadening factor and the refractive index exhibit similar anomalous temperature dependence. These results are consequences of carrier localization induced by potential fluctuation or possible other disorder mechanisms, such as phase separation and phase transition. By simulating the "semi-S-shaped" or "S-shaped" behavior of E_g by means of different models, we determine the magnitude of carrier localization in samples A and B to be about 11 and 40 meV, respectively.

Acknowledgments

The work is supported by Education Bureau of Sichuan Province, PR China (Project no. 2006B033). The authors would like to thank Prof. H.Z. Wu at Zhejiang University for the support of samples and Mr. Q. Deng for his technical help.

References

[1] T. Gruber, C. Kirchner, R. Kling, F. Reuss, A. Waag, Appl. Phys. Lett. 84 (2004) 5359.
[2] A. Ohtomo, M. Kawasaki, T. Koida, K. Masubuchi, H. Koinuma, Y. Sakurai, Y. Yoshida, T. Yasuda, Y. Segawa, Appl. Phys. Lett. 72 (1998) 2466.
[3] S. Choopun, R.D. Vispute, W. Yang, R.P. Sharma, T. Venkatesan, H. Shen, Appl. Phys. Lett. 80 (2002) 1529.
[4] J. Narayan, A.K. Sharma, A. Kvit, C. Jin, J.F. Muth, O.W. Holland, Solid State Commun. 121 (2002) 9.
[5] J. Chen, W.Z. Shen, N.B. Chen, D.J. Qiu, H.Z. Wu, J. Phys.: Condens. Matter 15 (2003) L475.
[6] J. Chen, W.Z. Shen, Appl. Phys. Lett. 83 (2003) 2154.
[7] Q. Li, S.J. Xu, W.C. Cheng, M.H. Xie, S.Y. Tong, C.M. Che, H. Yang, Appl. Phys. Lett. 79 (2001) 1810.
[8] R.W. Martin, P.G. Middleton, K.P. O'Donnell, W. Van der Stricht, Appl. Phys. Lett. 74 (1999) 263.
[9] K.B. Lee, P.J. Parbrook, T. Wang, F. Ranalli, T. Martin, R.S. Balmer, D.J. Wallis, J. Appl. Phys. 101 (2007) 053513.
[10] S.J. Chung, M. Senthil Kumar, H.J. Lee, E.-K. Suh, J. Appl. Phys. 95 (2004) 3565.
[11] A. Bell, S. Srinivasan, C. Plumlee, H. Omiya, F.A. Ponce, J. Christen, S. Tanaka, A. Fujioka, Y. Nakagawa, J. Appl. Phys. 95 (2004) 4670.
[12] S. Mazzucato, R.J. Potter, A. Erol, N. Balkan, P.R. Chalker, T.B. Joyce, T.J. Bullough, X. Marie, H. Carrère, E. Bedel, G. Lacoste, A. Arnoult, C. Fontaine, Physica E 17 (2003) 242.
[13] J. Huso, J.L. Morrison, H. Hoeck, E. Casey, L. Bergman, T.D. Pounds, M.G. Norton, Appl. Phys. Lett. 91 (2007) 111906.
[14] C.J. Pan, K.F. Lin, W.T. Hsu, W.F. Hsieh, J. Phys.: Condens. Matter 19 (2007) 186201.
[15] K. Koike, I. Nakashima, K. Hashimoto, S. Sasa, M. Inoue, M. Yano, Appl. Phys. Lett. 87 (2005) 112106.
[16] H.D. Sun, T. Makino, Y. Segawa, M. Kawasaki, A. Ohtomo, K. Tamuraand, H. Koinuma, J. Appl. Phys. 91 (2002) 1993.
[17] A. Satake, Y. Masumoto, T. Miyajima, T. Asatsuma, F. Nakamura, M. Ikeda, Phys. Rev. B 57 (1998) R2041.
[18] N.B. Chen, H.Z. Wu, D.J. Qiu, T.N. Xu, J. Chen, W.Z. Shen, J. Phys.: Condens. Matter 16 (2004) 2973.
[19] H.P. Zhou, W.Z. Shen, N.B. Chen, H.Z. Wu, Appl. Phys. Lett. 85 (2004) 3723.
[20] C.W. Teng, J.F. Muth, Ü. Özgür, M.J. Bergmann, H.O. Everitt, A.K. Sharma, C. Jin, J. Narayan, Appl. Phys. Lett. 76 (2000) 979.
[21] F.B. Naranjo, M.A. Sánchez-García, F. Calle, E. Calleja, B. Jenichen, K.H. Ploog, Appl. Phys. Lett. 80 (2002) 231.
[22] Y.P. Vaishni, Physica 34 (1967) 149.
[23] L. Vina, S. Logothetidis, M. Cardona, Phys. Rev. B 30 (1984) 1979.
[24] J.D. Baranovski, A.L. Efros, Sov. Phys. Semicond. 12 (1978) 1328.
[25] N. Nepal, J. Li, M.L. Nakarmi, J.Y. Lin, H.X. Jiang, Appl. Phys. Lett. 88 (2006) 062103.
[26] C.M. Jin, R.J. Narayan, J. Electron. Mater. 35 (2006) 869.